THE JOURNAL OF PHYSICAL CHEMISTRY C

Article

pubs.acs.org/JPCC

Measurement of Interlayer Screening Length of Layered Graphene by Plasmonic Nanostructure Resonances

Hsiang-An Chen,[†,○] Cheng-Lun Hsin,[‡,∥,○] Yu-Ting Huang,[⊥] Ming Lee Tang,[†] Scott Dhuey,[#] Stefano Cabrini,[#] Wen-Wei Wu,[⊥] and Stephen R. Leone*[,†,§,▽]

[†]Departments of Chemistry, [‡]Materials Science and Engineering, and [§]Physics, University of California, Berkeley, California 94720, United States

[∥]Department of Electrical Engineering, National Central University, Taoyuan 32001, Taiwan

[⊥]Department of Materials Science and Engineering, National Chiao Tung University, Hsinchu 30010, Taiwan

[#]Molecular Foundry and [▽]Chemical Sciences Division, Lawrence Berkeley National Laboratory, Berkeley, California 94720, United States

Supporting Information

ABSTRACT: The variation in localized surface plasmon resonances of single Au nanodisks (diameter 100 nm and height 25 nm) on 0−13 graphene layers is investigated using dark-field scattering spectroscopy to obtain the graphene electric field screening length. For nanodisks (NDs) with and without underlying graphene layers on a SiO_2 (300 nm)/Si substrate, the plasmon resonance red shifts from 604 to 620 nm with increasing graphene layers. The spectra of the plasmonic nanostructures obey an exponential saturation function versus increasing number of layers of graphene from 0 to 13. As a conducting film, the graphene layers screen the electric field generated by the plasmonic resonance of the Au NDs in the vicinity of the interface, and the red shifts of the resonance wavelength are explained in the framework of the electromagnetic field coupling between in-plane antiparallel image dipoles in the graphene layers and the ND dipole. A screening length of 1.2 ± 0.2 nm, equivalent to 3−4 graphene layers, is experimentally obtained, in good agreement with the measurement by field-effect transistors and theoretical calculation in doped graphene. The resonance shift of plasmonic nanostructures on a layered graphene system provides an alternative and convenient method for screening length measurement of graphene films.

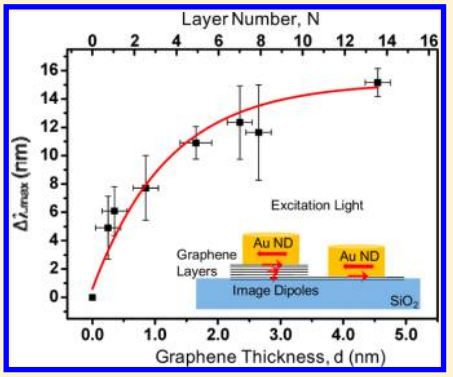

INTRODUCTION

In recent years, graphene, a single layer of honeycomb-lattice-arranged carbon atoms, has attracted intense interest in the development of graphene-based nanoelectronic devices due to its excellent mechanical, electrical, and thermal properties.[1,2] Single-layer graphene exhibits remarkably high electron mobility at room temperature and outstanding thermodynamic stability, leading to great potential for applications such as transparent conducting electrodes in solar cells and ultrafast photodetectors.[3,4] In stacked graphene multilayers, the tight-binding Hamiltonian describes hopping of electrons between neighboring sites, indicating the first nearest-neighbor hopping energy between carbon atoms within a given layer is t = 2.8 eV and the interlayer hopping between the nearest neighbors in adjacent layers is $t_\perp$ = 0.3 eV. As these hopping energies are proportional to the probability of electron hopping,[5] the electron transport in graphene multilayers is analyzed as independent graphene layers attached in parallel to a contact showing anisotropic properties due to the dominant intralayer electron hopping and minor interlayer hopping.[6] Also, the metallic nature and high carrier density of graphene layers cause electrostatic screening perpendicular to the layers in electrical devices, such as multilayered graphene field effect transistors (FETs).[6,7] According to previous reports, the screening length is described as a characteristic decay length of electromagnetic field or charge density, which decreases exponentially from the graphene surface layer. These thickness-dependent profiles are usually estimated versus the nanometer-scale film thickness or the number of graphene layers. The conversion between layer number and nanometer thickness is calculated from the single-layer graphene thickness of 0.34 nm estimated by optical measurement.[8] In a single-layer graphene FET, the electrical characteristics exhibit a substantial amount of noise at low temperature and room temperature.[9] Recent studies show that multilayered graphene employed for the FET channel material reduces the noise by restraining the effects of built-in electric fields from substrates.[6,7] Therefore, understanding the degree of interlayer screening is essential for many applications of multilayer graphene.

Special Issue: Ron Naaman Festschrift

Received: December 15, 2012
Revised: March 23, 2013
Published: March 25, 2013

dx.doi.org/10.1021/jp312363x | J. Phys. Chem. C 2013, 117, 22211−22217

Recently, several experimental approaches have been reported to quantify the interlayer screening of graphene layers. The interlayer screening lengths in multilayer graphene systems or thin graphite films were investigated by measurements of layer-dependent variations in several graphene properties. For example, the layer-dependent carrier concentration profiles caused by a built-in electric field at a SiC−graphene substrate interface were resolved by ultrafast mid-infrared pump−probe spectroscopy[10] and angle-resolved photoemission spectroscopy[11] and provided a direct estimate of screening lengths of 1 layer and 3−4 layers, respectively. Scanning probe techniques such as electrostatic force microscopy[12] and Kelvin probe force microscopy[13] were implemented to elucidate the interlayer screening effect of graphene by measuring surface potential variation as a function of layer number in gate device configurations. In another method using a top and bottom gate configuration in graphene FETs, a scan of the top gate voltage was applied to demonstrate a thickness dependence of the resistance peak shifted by the bottom voltage, finding the electric field was screened out with an interlayer screening length of 1.2 nm, namely, 3−4 layers of graphene.[14,15] The experimentally estimated screening length values, thus, range from about one single layer to several layers, i.e., values of 1−4. The wide range of the values might be attributed to the graphene stacking order, defects, doping, and charges trapped at the interface between the substrate and the graphene.[16,17] Theoretically obtained screening lengths also vary from a single layer to 3−5 layers under different assumptions. A theoretical screening length of 0.54 nm (1−2 layers of graphene) obtained by Visscher et al. was under the assumption that there is no interlayer electron tunneling and electronic hybridization between layers.[18] Guinea extended Visscher's model by considering the interlayer hopping and a tight-binding electronic structure model for π orbitals. A calculated charge distribution in an applied field indicates a screening length of 2−3 graphene layers in doped graphene systems.[19] Thus far, it is still challenging to obtain a complete theoretical description that considers all the parameters that affect the graphene screening values.

Here, we demonstrate an alternative and convenient method for screening length measurement of graphene layers by using plasmonic nanostructure resonances. When a coherent oscillation of conductive electrons, called a localized surface plasmon resonance (LSPR),[20] is excited in a metal nanostructure, the electromagnetic field in the vicinity of the nanostructure surface is strongly enhanced. Specific optical scattering, absorption, and extinction properties can be found in the corresponding spectra, and the peaks in the spectra, usually called LSPR peaks, are crucial in many applications such as surface-enhanced Raman spectroscopy[21,22] and SP resonance biosensors.[20,23] In our work, an array of uniform, lithographically prepared nanodisks (NDs) with and without underlying graphene layers on a SiO_2 (300 nm)/Si substrate are employed to investigate the interlayer screening effect of multilayered graphene on the electric fields generated by the ND plasmonic resonances using single nanodisk dark-field scattering spectroscopy. A screening length of 1.2 ± 0.2 nm, namely, 3−4 layers, is obtained by fitting the resultant resonance peak shift of the spectra of single NDs versus the thickness of the underlying graphene layers. The results are explained in the framework of the electromagnetic field coupling between in-plane antiparallel image dipoles in the graphene layers and the ND dipole.

EXPERIMENTAL SECTION

Graphene flake samples with sizes around 10 μm × 20 μm were prepared by mechanical exfoliation of highly oriented pyrolytic graphite (HOPG) on Si substrates with a 300 nm thick SiO_2 layer.[1] The thicknesses and layer numbers of the graphene flakes were characterized by atomic force microscopy (AFM, BioScope, Veeco) and Raman spectroscopy (INVIA Raman Spectrometer with 488 nm argon ion laser). For the fabrication of Au ND arrays, a poly(methylmethacrylate) (PMMA) film with a thickness of 50 nm was prepared on graphene sample substrates by spin-coating a solution of 1 wt % PMMA 950K in chlorobenzene and baking at 180 °C for 5 min. A Vistec VB300 e-beam lithography system was used to expose arrays of circular-shaped patterns of 100 nm in diameter and 1.5 or 2 μm spacing in the area where graphene layers were located. A careful and selected choice of electron beam dose is required to achieve a uniform size of the patterns. The patterns were developed using a high contrast cold development solution of 7:3 IPA:water at −5 °C ultrasonicated for 100 s. After 25 nm thick Au metal depositio nwithout adhesion layer by thermal evaporation and a PMMA lift-off process with dichloromethane, Au ND arrays were created. The size of the fabricated NDs was inspected with scanning electron microscopy (SEM, JSM-6340F, Jeol). The measurement of dark-field scattering spectroscopy was performed by a dark-field optical microscope (Axioplan 2 imaging, Zeiss) equipped with a dark-field objective (50×, NA = 0.5, Epiplan-NEOFLUAR, Zeiss) and a 50 W white-light source. The collected scattered light was guided into a spectrometer (Acton SpectraPro 2300i, Princeton Instruments) with a liquid-nitrogen-cooled charge-coupled device (CCD) detector. The spectra of the single NDs were obtained by measuring the signals from each ND, subtracting the background signals of the substrate nearby the ND, and normalizing by the intensity of incident light. The spectrum measurement was implemented with an exposure time of ∼1 s and, averaging 30 such spectra, carried out in the dark to reduce the random noise effectively. The standard deviation of the resonant scattering peak relevant to the measurement system was estimated to be ∼0.3 nm by repeated measurements of a single ND. The deviation is small compared to the spectral shifts versus graphene layer thickness. In addition, the overall deviation in single ND scattering peaks should be dominated by the deviation of the fabricated dimension of each ND. Limited to the area sizes of graphene, the spectra corresponding to the NDs on specific layer numbers of graphene were collected from at least three and up to eight NDs in our work for analysis.

RESULTS AND DISCUSSION

Figure 1a shows the SEM image of a ND array fabricated by e-beam lithography on a SiO_2 (300 nm)/Si substrate. The NDs have a circular shape with a size of 100 ± 2.5 nm in diameter and a spacing of 2 μm, and the thickness of the NDs is 25 ± 1 nm, confirmed by AFM measurement (see Supporting Information SI1). For optical characterization, a 1.5 μm wide slit is implemented before the spectrometer, which allows the scattered light from one column of the NDs to be detected and imaged by the CCD in the spectrometer, as shown in Figure 1b. In Figure 1c, each bright-colored line represents the corresponding LSPR scattering spectra of the single NDs shown in Figure 1b, and as can be seen, the NDs exhibit single-peak scattering spectra that have an average resonance peak wavelength at 604.5 nm with a standard deviation of 2.4 nm.

dx.doi.org/10.1021/jp312363x | J. Phys. Chem. C 2013, 117, 22211−22217

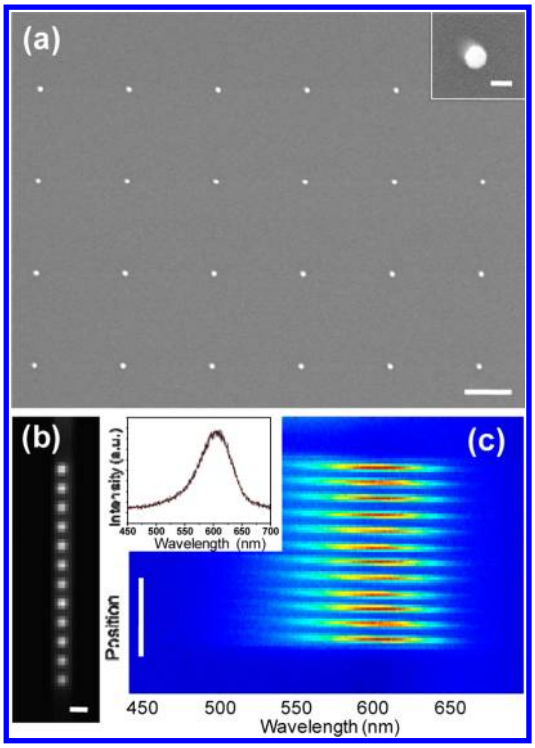

Figure 1. (a) SEM image of a Au ND array with an average diameter of 100 ± 2.5 nm, and the inset in (a) is an enlarged view of a ND. (b) The dark-field optical image of one of the ND columns in the array, recorded by the CCD under image mode of the spectrometer. (c) The corresponding scattering spectra of the single NDs in (b) with an average resonance peak at 604.5 ± 2.4 nm; the red color represents the greatest intensity. The inset in (c) is one of the single ND scattering spectra. Scale bars in (a), (b), (c) and inset in (a) are 1 μm, 2 μm, 10 μm, and 100 nm, respectively.

One of the single ND scattering spectra is shown in the Figure 1c inset. The small deviation of resonance peaks reveals a good uniformity of the fabricated NDs, which is an important premise for the following experiment.

Samples with Au ND arrays fabricated by e-beam lithography on mechanically exfoliated graphene flakes are shown in Figure 2a,b. The darker the color of the graphene flakes seen in the optical images, the thicker they are.[8,24] Figure 2c shows the topographic image of the graphene flake corresponding to the red square in Figure 2a obtained by tapping mode AFM measurement. The thickness of the upper part of the graphene flake is measured to be 0.8−0.9 nm. The corresponding Raman spectrum as shown in the top blue line in Figure 2d confirms that it is a single-layer graphene by the very low G-band (1584 cm^{-1}) intensity and the symmetric and sharp 2D-band (~2670 cm^{-1}).[21,22] Thus, the graphene layer number, N, can be estimated by the AFM measured thickness $T_{AFM} = 0.8 + (N - 1) \times 0.34$ in units of nanometers, where 0.34 nm is the theoretical thickness for one layer of graphene and 0.8 nm is the layer thickness of the first layer graphene interacting with the SiO_2 substrate. Various studies of AFM thickness measurements for graphene layers have reported an additional offset of 0.3−0.55 nm for the distance between the first-layer graphene and SiO_2 substrate due to the adsorbed water vapor that remains captured between graphene and SiO_2.[1,25] The Raman spectra of 2, 5, and 13 graphene layers determined by AFM measured thicknesses are shown in the rest of Figure 2d. For the samples of two and five layers of graphene, the Raman

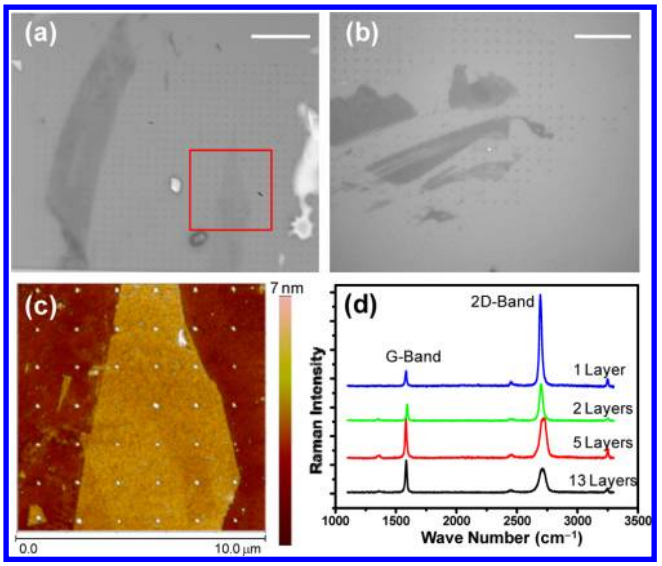

Figure 2. (a) and (b) Optical images of mechanically exfoliated graphene flakes with the fabricated Au ND arrays. (c) The AFM image of the graphene layer corresponding to the square in (a). (d) The Raman spectra of graphene ranging from 1 to 13 layers. Scale bars in (a) and (b) are both 10 μm.

D-band peak at 1365 cm^{-1} appears, which indicates the existence of the defect.[21,22] The presence of the D band could be attributed to intrinsic defects in the graphite before transferring the graphene to the substrate. Also, it is suggested that some wrinkles or extrinsic defects may be introduced randomly during the transfer of the graphene layers onto the SiO_2/Si substrates by using the mechanical exfoliation method on these samples.

As shown in Figure 3a, five NDs, located directly on SiO_2 and on graphene layer numbers of 1, 5, 7, and 13, exhibit a

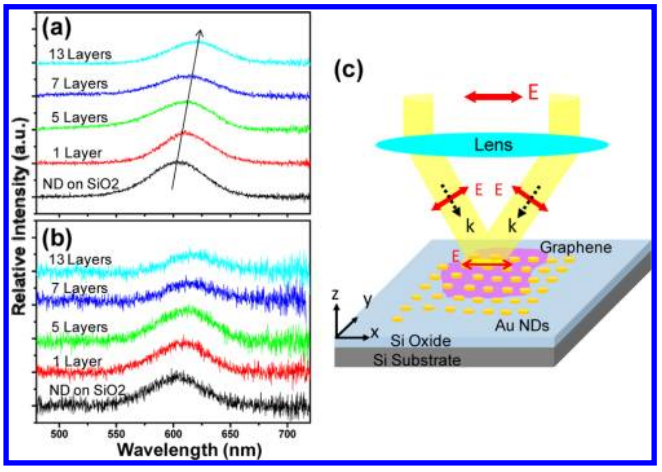

Figure 3. Scattering spectra of single NDs without and with underlying graphene of 1, 5, 7, and 13 layers on SiO_2(300 nm)/Si substrates under (a) unpolarized and (b) parallel-polarization incident excitation. (c) A schematic diagram of scattering measurement under dark-field mode.

distinct red-shift of the scattering resonance peak from 604 to 620 nm, measured with a configuration of dark-field microscopy as in Figure 3c under unpolarized incident light. Recent studies of the electromagnetic field coupling between metal nanoparticles and metal films have reported that the

dx.doi.org/10.1021/jp312363x | J. Phys. Chem. C 2013, 117, 22211−22217

nanoparticles can be approximated as a point dipole oscillator, and the metal films act like a mirror with an image dipole lying in the metal.[26−28] Since graphene layers are similar to metallic conductive films, the spectral shifts in Figure 3a can be explained by the coupling between the ND dipole and its image dipoles created in the different layer numbers of the graphene. In the case of Au nanoparticles on a metal film under parallel polarized excitation (polarization parallel to the interface of the substrate and the nanoparticle, such as along the x or y direction in Figure 3c),[29,30] the image dipoles in the metal film are induced by the laterally oscillating dipoles (e.g., in $+x$ direction) in Au nanoparticles and couple in the plane but with an opposite dipole direction (in $-x$ direction); namely, it is antiparallel dipole coupling that tugs on the plasmonic oscillation of the nanoparticle dipoles and leads to a red shift of the resonance peak and cancellation of the total scattering of Au nanoparticles causing weaker spectral features. In contrast, under perpendicularly polarized excitation (polarization perpendicular to the interface of the substrate and the nanoparticle, namely, along the z direction in Figure 3c), the induced dipoles in the metal film and the Au nanoparticle dipoles are vertically oscillating dipoles in the same direction as the coupling (e.g., both in $+z$ direction), which would yield a much higher scattering and contributes to a different peak shift from the one that is excited by the parallel polarization.[29,30] Here, in our experiment, by placing a linear polarizer between the light source and the microscope objective in the dark-field microscopy setup in Figure 3c, the incoming ring-shaped light (annular illumination) created by a circular light stop is focused onto the sample with an approximately constant tilted angle of 30° to the perpendicular of the surface due to the lens (50×, NA = 0.5). The polarization of the light was not affected, as the light is focused on the substrate with the tilted angle of 30°, and there is a pure electric field parallel to the substrate surface, namely, along the x direction in Figure 3c (see Supporting Information SI2).[31] To specify the oscillation component of the image dipoles, in Figure 3b, the parallel polarized light is incident on the sample for the scattering spectra of the same five NDs as measured in Figure 3a, and there are nearly unchanged resonance peak positions from 604 to 620 nm.

The result of a nearly unchanged red-shift of resonance peaks indicates that under unpolarized excitation dominant laterally oscillating image dipoles (along the x direction) are induced in graphene layers by the ND dipoles, which have both lateral (along the x or y direction) and vertical dipole oscillation (along the z direction). This matches the expected strongly anisotropic properties of graphene layers, namely, more conductive in the parallel direction of layers. Also, the spectral intensities in Figure 3a,b are the result of the normalization by their unpolarized and polarized incident light intensities, respectively. As can be seen, the scattering spectra under polarized excitation suffer a worse signal-to-noise ratio than the unpolarized spectra. Since there is less incident intensity in the polarized excitation, the overall scattering signals are weaker. The line widths in the spectra are randomly distributed in the range of 55−62 nm, and an observable intensity reduction is observed for graphene of more than five layers, especially in the parallel polarized case. The results suggest that antiparallel image dipoles reduce the plasmonic radiation of the NDs as the layer number is increasing. In addition, the unchanged spectral peak for Au NDs on SiO_2 under unpolarized and polarized excitation is rational since SiO_2 is a low-index substrate having no mirror effect for coupling.

To understand the relationship between the peak shift and the thickness of the graphene layers, we collected several sets of unpolarized scattering spectra from single NDs above graphene with different layer numbers. The LSPR peak shift versus the thickness of graphene is shown in Figure 4a. The $\Delta\lambda_{max}$

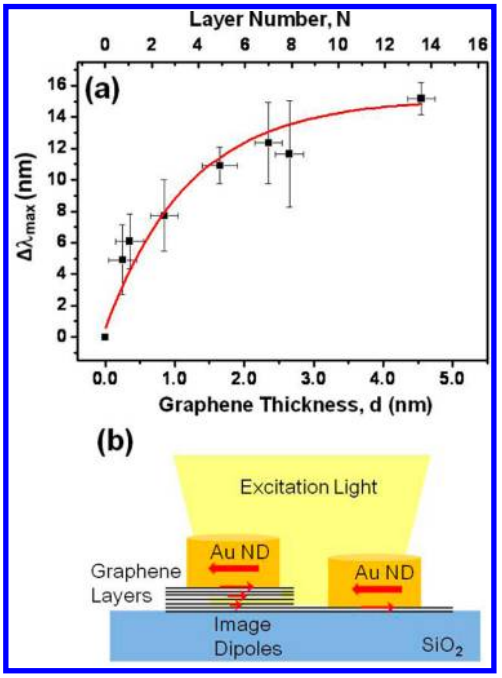

Figure 4. (a) Plot of the LSPR peak shift of the single NDs versus the corresponding underlying graphene thickness with a fitting curve, red line, by using the exponential equation. (b) Schematic of the coupling between ND dipoles and antiparallel image dipoles in different graphene layers (not to scale) under incident light. The error bars in (a) are about ±0.2 nm for thickness and 1−3.3 nm for the resonance peak shift.

corresponding to each point in the plot is an average from at least three and up to eight single ND spectra, with standard deviations of 1−3.3 nm; the AFM thickness fluctuation measurement is assessed to be accurate to ±0.2 nm by scanning a calibration sample. The reference $\Delta\lambda_{max} = 0$ is defined by the average resonance peak observed at 604 nm for Au NDs on SiO_2, and the measured thickness of the graphene layers by AFM are all offset with a subtraction of 0.5 nm. The reason for the thickness modification is that a single layer of graphene sheet on the SiO_2 is obtained by AFM at 0.8−0.9 nm due to the first graphene layer interacting with SiO_2. Therefore, a subtraction offset of 0.5 nm allows the layered graphene systems to fit the theoretical thickness of 0.34 nm for each layer of graphene. As can be seen in Figure 4a, the red shift of the resonance wavelength, $\Delta\lambda_{max,}$ follows an exponential saturation function versus graphene thickness, d, ascending from 0.34 ± 0.2 nm to 4.55 ± 0.2 nm; namely, layer numbers of graphene increase from 1 to 13. In many cases,[32,33] refractive index sensing in the short-range (less than 100 nm) region by metal nanostructures can be approximated by a model for the effect on surface plasmons based on a planar metal surface in which the electric field in the metal decays exponentially over a length scale of around 50−100 nm in the different dielectric material. In the case of a Au core with a dielectric shell of varying thickness of less than 2 nm, the LSPR peak wavelength linearly shifts to the red with respect to the shell thickness. For a shell

dx.doi.org/10.1021/jp312363x | J. Phys. Chem. C 2013, 117, 22211−22217

with increasing thickness up to ~60 nm, the wavelength shift decreases exponentially and saturates.[33] An empirical equation reported in refs 32 and 33 that describes the peak wavelength shift versus the thickness of the refractive index change is written as

$$\Delta\lambda_{max} = m\Delta n[1 - \exp(-d/L_d)]$$

where Δn is the difference between the refractive index of the sensing material and the surrounding medium; m is the refractive index sensitivity $\Delta\lambda_{max}/\Delta n$ measured from the different uniform refractive index medium at a saturated sensing thickness; d is the thickness of the sensing material; and L_d is the characteristic decay length of the electromagnetic field surrounding the plasmonic nanostructures. As $d < 2$ nm, the exponential equation can be reduced to a linear function, which agrees with the case of an extremely thin shell for the sensing. In our case, the complex refractive index of graphene in the visible region can be described regardless of layer numbers of graphene by $n = 3.0$ and $k = (C_1/3)\lambda$; here C_1 is a constant value in Bruna et al.[34] According to the constant real part of the refractive index, $n = 3$, for varying layers of graphene, we consider that $m\Delta n$ is a constant, and there are two free parameters, the $\Delta\lambda_{max}$ (resonance peak shift) and d (the graphene thickness), for this equation. By using this equation, a curve with $m\Delta n = 15.2$ nm and an electric field decay length of $L_d = 1.2 \pm 0.2$ nm gives a good fit to the experimental data as shown in Figure 4a. The much smaller values of $m\Delta n$ and L_d in our case, compared to $m\Delta n = 100-150$ nm and $L_d = 10-20$ nm, in the case of a nanoparticle surrounded by dielectric,[32,33] indicate that the strength of the electric field decreases tremendously when penetrating into the graphene layers, which results from the large graphene metallic screening effect. The obtained electric field decay length of $L_d = 1.2 \pm 0.2$ nm (layer numbers, $N = 3-4$, red line in Figure 4a), namely, the screening length of graphene, is in good agreement with the measurement by FETs, which gives a screening length of 1.2 nm,[14,15] and with theoretical calculation in doped graphene which gives a screening length of 2−3 layers.[19]

The resonance shifts in the systems of metal nanoparticles on a metal film are often analyzed based on an approximate nanoparticle point dipole located at the center of the nanoparticle and are discussed in terms of the classical image-dipole model.[27,28] In the classical image-dipole model, the induced dipoles in the metal film may have the identical (for perpendicular polarization coupling) or opposite (for parallel polarization coupling) directions relative to the nanoparticle dipoles, and both are located at the same distance to the interface between the nanoparticle and the metal film. However, in our work, the thicknesses of the graphene layers are much smaller than the height of the NDs, and this means that the classical point dipole approximation is not suitable for our system. Recently, Lee et al. observed that the surface potential gradient exponentially decreases in graphene multilayers resulting from the independent screening of the surface potential layer by layer.[13] Kuroda and Datta et al. found a nonexponential (approximate power-law) decay of induced carrier density profile through the layers of the graphene system subjected to a gate bias.[12,35] According to those studies, here we deduce a similar model for the coupling of the ND dipole and image dipoles in multiple graphene layers as expressed in Figure 4b of the schematic. Typically, a dipole field falls off as the inverse cube of distance (r^{-3}), and the induced dipole moment would show a linear response to the field.[36] Thus, the image dipole moments in graphene layers were suggested to possess an approximate power-law decay function of the distance away from the ND. Due to the screening effect in graphene, the two opposite electric fields corresponding to the ND dipole and the image dipole would be partially counterbalanced, and the overall electric field in graphene layers is approximated as an exponential decay.[12,13] According to ref 37, the two plasmonic dipole coupling system was estimated to be an exponential function versus distance. In our case, the overall dipole coupling in multilayers of graphene needs to be the integral of dipole coupling of each layer through the graphene layer thickness. Since the exponential function after the integral would still remain as an exponential form for the overall dipole coupling, this corresponds well with the observation of exponential saturation of $\Delta\lambda$ with the graphene thickness, as shown in Figure 4a and described by the fitting equation.

In our experiment, there are some factors that might affect the screening length estimation. For example, the Au is deposited at a relatively low temperature and does not undergo any high-temperature annealing to avoid a possible nanodisk shape change and Au diffusion into graphene. Therefore, the Au nanodisks should only be connected to the topmost layer of graphene without severe diffusion, which might cause compound generation. There is little PMMA contamination residual by using dichloromethane as lift-off solvent as confirmed by Raman spectra (see Supporting Information SI3). Therefore, we assume that the Au and graphene are in clean contact and without intercalation.[38] The binding between Au and graphene was reported to be relatively weak, i.e., a physical adsorption,[17] compared to the chemisorption of Co, Ni, and Ti metals, which perturb the electronic structure of graphene strongly. Although the binding is weak, the Fermi-level shift of "physisorbed" graphene has been predicted to be around 0.19 eV as p-doped by Au metal.[17,38] Thus, our Au NDs were expected to alter the carrier concentration of graphene, as well as the strength of induced image dipoles here, thus altering the screening length from the neutral graphene system. The less-doped graphene multilayers have larger screening lengths due to the weaker carrier screening capability.[11] In addition, there is another factor; there might be a relatively small air gap between the Au grains and the topmost graphene. In ref 38, the separation between the carbon atoms and the Au atoms at the interface of the Au−graphene contact has been predicted to have an effect of a Fermi-level shift of graphene. The calculation postulates the Fermi-level shift increases from 0.19 to 0.35 eV (more doped) as the separation varies from the equilibrium separation of 3.3 Å to an out-of-equilibrium separation of 4 Å. We can use the above concepts to estimate the screening length variation trend by the doping condition. Once the air gap is too large to form adsorption binding between Au and graphene, the electric field generated by the Au NDs would barely decay through the air gap and reach the topmost graphene layer with nearly an unchanged electric field strength due to the low dielectric constant of air, $\varepsilon_{air} = 1$, but without any metal-doping effect. The subtraction offset in the AFM measured thickness is a reasonable assumption because we are focusing on the actual thickness of graphene that screens the electric field. Therefore, the additional thickness caused by the interaction between SiO_2 and the first layer of graphene would be eliminated. Other facts such as the uniformity of the Au NDs and the fluctuation of the spectral and AFM measurements can be carefully evaluated to reach a precise screening length measurement.

dx.doi.org/10.1021/jp312363x | J. Phys. Chem. C 2013, 117, 22211−22217

CONCLUSIONS

In summary, we studied the variation in localized surface plasmon resonances of single Au NDs on graphene multilayers using dark-field scattering spectroscopy, and the plasmonic nanostructures provide an exponential saturation function of the resonance peak shift versus the thickness of underlying graphene. Red shifts of the resonance wavelength are explained in the framework of the electromagnetic field coupling between the ND dipole and the in-plane antiparallel image dipoles in the graphene layers originating from the interlayer screening effect. A screening length of 1.2 ± 0.2 nm equivalent to 3−4 graphene layers is experimentally obtained, which is in good agreement with the measurement by FETs and theoretical calculations in doped graphene. The resonance shift of plasmonic nanostructures on a layered graphene system can be an alternative and convenient method for the screening length measurement of graphene films.

ASSOCIATED CONTENT

Supporting Information

(SI1) The cross-sectional line scan profile corresponds to Figure 2c obtained by AFM measurement. (SI2) Calculation of the polarization of the incident electric field. (SI3) Raman spectra for graphene after PMMA removal by dichloromethane and acetone. This material is available free of charge via the Internet at http://pubs.acs.org.

AUTHOR INFORMATION

Corresponding Author

*Phone: (510) 643-5467. E-mail: srl@berkeley.edu.

Author Contributions

○These authors contributed equally to this work.

Notes

The authors declare no competing financial interest.

ACKNOWLEDGMENTS

The authors acknowledge Sarah Brittman for technical assistance and Terefe G. Habteyes for valuable discussions. This work is supported by a National Security Science and Engineering Faculty Fellowship, Air Force Office of Scientific Research under Grant No. AFOSR-NSSEFF-FA9550-10-1-0195, and postdoctoral research abroad program, National Science Council, Taiwan, under Contract No. NSC100-2917-I-564-056. Supplies and equipment are provided through the Materials Science Division (MSD) and Molecular Foundry, Lawrence Berkeley National Laboratory (LBNL), through support of the Director, Office of Science, Office of Basic Energy Sciences, Chemical Sciences Division of the U.S. Department of Energy under Contract No. DE-AC02-05CH11231. Portions of the experimental supplies are provided by Cheng-Lun Hsin and Wen-Wei Wu under National Science Council, Taiwan, Grant No. NCS 101-2218-E-008-014-MY2 and No. NSC 100-2628-E-009-023-MY3, respectively.

REFERENCES

(1) Novoselov, K. S.; Geim, A. K.; Morozov, S. V.; Jiang, D.; Zhang, Y.; Dubonos, S. V.; Grigorieva, I. V.; Firsov, A. A. Electric Field Effect in Atomically Thin Carbon Films. *Science* **2004**, *306*, 666−669.

(2) Avouris, P. Graphene: Electronic and Photonic Properties and Devices. *Nano Lett.* **2010**, *10*, 4285−4294.

(3) Xia, F. N.; Mueller, T.; Lin, Y. M.; Valdes-Garcia, A.; Avouris, P. Ultrafast Graphene Photodetector. *Nat. Nanotechnol.* **2009**, *4*, 839−843.

(4) Kasry, A.; Kuroda, M. A.; Martyna, G. J.; Tulevski, G. S.; Bol, A. A. Chemical Doping of Large-Area Stacked Graphene Films for Use as Transparent, Conducting Electrodes. *ACS Nano* **2010**, *4*, 3839−3844.

(5) Tabert, C. J.; Nicol, E. J. Dynamical Conductivity of AA-Stacked Bilayer Graphene. *Phys. Rev. B* **2012**, *86*, 075439.

(6) Sui, Y.; Appenzeller, J. Screening and Interlayer Coupling in Multilayer Graphene Field-Effect Transistors. *Nano Lett.* **2009**, *9*, 2973−2977.

(7) Chen, J. H.; Jang, C.; Xiao, S. D.; Ishigami, M.; Fuhrer, M. S. Intrinsic and Extrinsic Performance Limits of Graphene Devices on SiO_2. *Nat. Nanotechnol.* **2008**, *3*, 206−209.

(8) Roddaro, S.; Pingue, P.; Piazza, V.; Pellegrini, V.; Beltram, F. The Optical Visibility of Graphene: Interference Colors of Ultrathin Graphite on SiO_2. *Nano Lett.* **2007**, *7*, 2707−2710.

(9) Ozyilmaz, B.; Jarillo-Herrero, P.; Efetov, D.; Kim, P. Electronic Transport in Locally Gated Graphene Nanoconstrictions. *Appl. Phys. Lett.* **2007**, *91*, 192107.

(10) Sun, D.; Divin, C.; Berger, C.; de Heer, W. A.; First, P. N.; Norris, T. B. Spectroscopic Measurement of Interlayer Screening in Multilayer Epitaxial Graphene. *Phys. Rev. Lett.* **2010**, *104*, 136802.

(11) Ohta, T.; Bostwick, A.; McChesney, J. L.; Seyller, T.; Horn, K.; Rotenberg, E. Interlayer Interaction and Electronic Screening in Multilayer Graphene Investigated with Angle-Resolved Photoemission Spectroscopy. *Phys. Rev. Lett.* **2007**, *98*, 206802.

(12) Datta, S. S.; Strachan, D. R.; Mele, E. J.; Johnson, A. T. C. Surface Potentials and Layer Charge Distributions in Few-Layer Graphene Films. *Nano Lett.* **2009**, *9*, 7−11.

(13) Lee, N. J.; Yoo, J. W.; Choi, Y. J.; Kang, C. J.; Jeon, D. Y.; Kim, D. C.; Seo, S.; Chung, H. J. The Interlayer Screening Effect of Graphene Sheets Investigated by Kelvin Probe Force Microscopy. *Appl. Phys. Lett.* **2009**, *95*, 222107.

(14) Miyazaki, H.; Li, S. L.; Kanda, A.; Tsukagoshi, K. Resistance Modulation of Multilayer Graphene Controlled by the Gate Electric Field. *Semicond. Sci. Technol.* **2010**, *25*, 034008.

(15) Miyazaki, H.; Odaka, S.; Sato, T.; Tanaka, S.; Goto, H.; Kanda, A.; Tsukagoshi, K.; Ootuka, Y.; Aoyagi, Y. Inter-Layer Screening Length to Electric Field in Thin Graphite Film. *Appl. Phys. Express* **2008**, *1*, 034007.

(16) Koshino, M. Interlayer Screening Effect in Graphene Multilayers with ABA and ABC Stacking. *Phys. Rev. B* **2010**, *81*, 125304.

(17) Khomyakov, P. A.; Giovannetti, G.; Rusu, P. C.; Brocks, G.; van den Brink, J.; Kelly, P. J. First-Principles Study of the Interaction and Charge Transfer between Graphene and Metals. *Phys. Rev. B* **2009**, *79*, 195425.

(18) Visscher, P. B.; Falicov, L. M. Dielectric Screening in a Layered Electron Gas. *Phys. Rev. B* **1971**, *3*, 2541−2547.

(19) Guinea, F. Charge Distribution and Screening in Layered Graphene Systems. *Phys. Rev. B* **2007**, *75*, 235433.

(20) Haes, A. J.; Stuart, D. A.; Nie, S. M.; Van Duyne, R. P. Using Solution-Phase Nanoparticles, Surface-Confined Nanoparticle Arrays and Single Nanoparticles as Biological Sensing Platforms. *J. Fluoresc.* **2004**, *14*, 355−367.

(21) Heeg, S.; Fernandez-Garcia, R.; Oikonomou, A.; Schedin, F.; Narula, R.; Maier, S. A.; Vijayaraghavan, A.; Reich, S. Polarized Plasmonic Enhancement by Au Nanostructures Probed through Raman Scattering of Suspended Graphene. *Nano Lett.* **2013**, *13*, 301−308.

(22) Schedin, F.; Lidorikis, E.; Lombardo, A.; Kravets, V. G.; Geim, A. K.; Grigorenko, A. N.; Novoselov, K. S.; Ferrari, A. C. Surface-Enhanced Raman Spectroscopy of Graphene. *ACS Nano* **2010**, *4*, 5617−5626.

(23) Hutter, E.; Fendler, J. H. Exploitation of Localized Surface Plasmon Resonance. *Adv. Mater.* **2004**, *16*, 1685−1706.

(24) Nair, R. R.; Blake, P.; Grigorenko, A. N.; Novoselov, K. S.; Booth, T. J.; Stauber, T.; Peres, N. M. R.; Geim, A. K. Fine Structure

Constant Defines Visual Transparency of Graphene. *Science* **2008**, *320*, 1308−1308.
(25) Gupta, A.; Chen, G.; Joshi, P.; Tadigadapa, S.; Eklund, P. C. Raman Scattering from High-Frequency Phonons in Supported N-Graphene Layer Films. *Nano Lett.* **2006**, *6*, 2667−2673.
(26) Pinchuk, A.; Hilger, A.; von Plessen, G.; Kreibig, U. Substrate Effect on the Optical Response of Silver Nanoparticles. *Nanotechnology* **2004**, *15*, 1890−1896.
(27) Mubeen, S.; Zhang, S. P.; Kim, N.; Lee, S.; Kramer, S.; Xu, H. X.; Moskovits, M. Plasmonic Properties of Gold Nanoparticles Separated from a Gold Mirror by an Ultrathin Oxide. *Nano Lett.* **2012**, *12*, 2088−2094.
(28) Hu, M.; Ghoshal, A.; Marquez, M.; Kik, P. G. Single Particle Spectroscopy Study of Metal-Film-Induced Tuning of Silver Nanoparticle Plasmon Resonances. *J. Phys. Chem. C* **2010**, *114*, 7509−7514.
(29) Okamoto, T.; Yamaguchi, I. Optical Absorption Study of the Surface Plasmon Resonance in Gold Nanoparticles Immobilized onto a Gold Substrate by Self-Assembly Technique. *J. Phys. Chem. B* **2003**, *107*, 10321−10324.
(30) Niu, J.; Shin, Y. J.; Lee, Y.; Ahn, J. H.; Yang, H. Graphene Induced Tunability of the Surface Plasmon Resonance. *Appl. Phys. Lett.* **2012**, *100*, 061116.
(31) Chen, H.-A.; Lin, H.-Y.; Lin, H.-N. Localized Surface Plasmon Resonance in Lithographically Fabricated Single Gold Nanowires. *J. Phys. Chem. C* **2010**, *114*, 10359−10364.
(32) Malinsky, M. D.; Kelly, K. L.; Schatz, G. C.; Van Duyne, R. P. Chain Length Dependence and Sensing Capabilities of the Localized Surface Plasmon Resonance of Silver Nanoparticles Chemically Modified with Alkanethiol Self-Assembled Monolayers. *J. Am. Chem. Soc.* **2001**, *123*, 1471−1482.
(33) Rindzevicius, T.; Alaverdyan, Y.; Kall, M.; Murray, W. A.; Barnes, W. L. Long-Range Refractive Index Sensing Using Plasmonic Nanostructures. *J. Phys. Chem. C* **2007**, *111*, 11806−11810.
(34) Bruna, M.; Borini, S. Optical Constants of Graphene Layers in the Visible Range. *Appl. Phys. Lett.* **2009**, *94*, 031901.
(35) Kuroda, M. A.; Tersoff, J.; Martyna, G. J. Nonlinear Screening in Multilayer Graphene Systems. *Phys. Rev. Lett.* **2011**, *106*, 116804.
(36) Griffiths, D. J. *Introduction to Electrodynamics*; Prentice-Hall International, Inc.: New Jersey, U.S., 1999; pp 110−159.
(37) Funston, A. M.; Novo, C.; Davis, T. J.; Mulvaney, P. Plasmon Coupling of Gold Nanorods at Short Distances and in Different Geometries. *Nano Lett.* **2009**, *9*, 1651−1658.
(38) Malec, C. E.; Davidovic, D. Electronic Properties of Au-Graphene Contacts. *Phys. Rev. B* **2011**, *84*, 033407.